Article citation info:
Rutkowska-Gorczyca M, Dziubek M, Wiśniewski M. Response of hydrogen charging diffusion of the austenitic stainless steel AISI 310s. Combustion Engines. 2024;198(3):68-73. https://doi.org/10.19206/CE-186591

Małgorzata RUTKOWSKA-GORCZYCA
Mateusz DZIUBEK
Marcin WIŚNIEWSKI

Combustion Engines
Polish Scientific Society of Combustion Engines

Response of hydrogen charging diffusion of the austenitic stainless steel AISI 310s

ARTICLE INFO

Received: 11 July 2023
Revised: 28 March 2024
Accepted: 28 March 2024
Available online: 4 June 2024

The subject of hydrogen embrittlement seems to be more and more up-to-date and needed to be explored. World research teams working on this issue have not developed a clear method of preventing this process. The conclusion is that this issue should be approached individually, depending on the type of material, its structure and operating conditions. The problem will escalate in the near future as a result of the planned replacement of the traditional energy sources used so far with hydrogen energy. The paper presents the method of electrochemical hydrogenation, which reflects the conditions of galvanic coating of metallic materials used in the automotive industry. The aim of the research was to determine the influence of the time of hydrogenation on the properties and microstructure of austenitic steel.

Key words: *hydrogen embrittlement, metallic materials, potentiostatic tests*

1. Introduction

The presence of hydrogen in metallic materials may result in a decrease in plasticity and the formation of locally brittle damage, in a phenomenon called hydrogen embrittlement (HE) [4, 5, 9, 13, 16, 17, 20]. This phenomenon, despite the huge amount of research devoted to it, has still not been fully explained. The mechanism of the negative impact of hydrogen on mechanical properties still requires precise explanations. Research and tests to determine the impact of the chemical composition and microstructure of steel on degradation caused by the presence of a corrosive environment will enable the correct selection of materials for specific hydrogen applications. Hydrogen embrittlement (HE) represents the deterioration of the mechanical properties of metals and alloys due to the presence of dissolved hydrogen in the lattice. The hydrogen embrittlement results in the loss of ductility, the decrease of fracture toughness, the increase in fatigue fracture growth rate, and brittle fracture failure in steel at low or subcritical stress levels. The fatigue behavior of hydrogen embrittled steel, including the fracture toughness, fatigue crack growth rate, fatigue life, and fracture surface or crack morphology, has been studied extensively in many research centers. The source of hydrogen supply to the metal is mainly hydrogen, which can enter the steel as a result of exposure to a hydrogen-rich gaseous environment at high pressure or by cathodic charging.

Nowadays, advanced research is being carried out on alternative, innovative ways to reduce the negative impact of transport on exhaust emissions into the environment [15]. One of the researched solutions that is gaining more and more attention is the use of hydrogen-powered internal combustion engines. Hydrogen engines open new perspectives for the automotive sector, but also pose new construction problems to be solved. A direct threat resulting in damage to engine components operating in a hydrogen environment is the phenomenon of hydrogen embrittlement of the material. This important issue results in a weakening of the material structure and an increase in susceptibility to cracking [12]. Especially this problem applies to metal materials. Hydrogen, which is the smallest known atom, has the ability to penetrate the metal structure. This is due to the diffusion of hydrogen into the material, which results in changes in the crystal structure of the material. As a result, the internally rebuilt material has a greater tendency to crack under load and brittleness.

Various materials are used for the construction of motors, depending on the requirements of the characteristics of the elements and the working conditions of the motor [7, 20–22, 25]. One of the groups of materials used due to their high strength and corrosion resistance are austenitic steels. The study of different grades of this stainless-steel aims to understand the influence of the hydrogen element on the structure and properties of the steel [1–3, 6, 8, 10–12, 14, 18, 19, 22, 23, 28]. Hydrogen embrittlement in austenite steels causes a change in strength parameters, therefore an important aspect in designing is the appropriate study of materials that will be selected as materials cooperating in the H_2 environment. AISI 310s heat resistant steel is an austenitic chromium-nickel grade with increased nickel content, showing high strength, ductility, resistance in air and oxidizing atmosphere to high temperatures up to 1050°C. Steel is used for mechanically loaded parts that work at high temperatures. Incorrect technological processes and working conditions at elevated temperatures can cause the formation of hard phases in austenitic steels. Depending on the chemical composition of the steel, $M_{23}C_6$ carbides may form [4, 10, 24–26].

Numerous literature items contain studies on the effect of heat treatment on the properties of materials made of austenitic steels. Long-term exposure to these steels at elevated temperatures (500–900°C) leads to the release of structural components by diffusion, which leads to a significant reduction in physical, chemical, and mechanical properties. Austenitic steels tend to form carbides along grain boundaries at elevated temperatures, this is called sensitization of the steel. In such a material, the grain boundary zone is depleted in chromium and more susceptible to intergranular corrosion and deformation-induced martensite formation.

This paper presents an analysis of the effect of the time of hydrogenation during electrolytic current processes on the microstructure, strength and hardness of metallic membranes made of heat sensitized AISI 310s steel. The steel was sensitized to the possibility of the presence of an alloyed austenite structure with $M_{23}C_6$ carbide precipitates, intended to simulate the conditions of incorrectly conducted welding processes or unfavorable operating conditions.

2. Materials and methodology

2.1. Steel AISI 310s

The material in the form of commercially available AISI 310s steel was selected for the tests. The tested steel showed a microstructure, equiaxed alloy austenite grains with precipitations of carbides forming a shell at the grain boundaries (Fig. 1). In the delivery state, according to the supplier, the material was characterized by the chemical composition given in Table 1. and showed the properties presented in Table 2. Membranes for the tests were prepared in the form of plates with a thickness of 0.7 mm, dimensions shown in Fig. 2. The area of interaction with the electrolyte during electrochemical processes was about 550 mm^2 and was the same for each sample. The surface of the materials before the electrochemical process was cleaned in an ultrasonic scrubber in an acetone solution for 10 min.

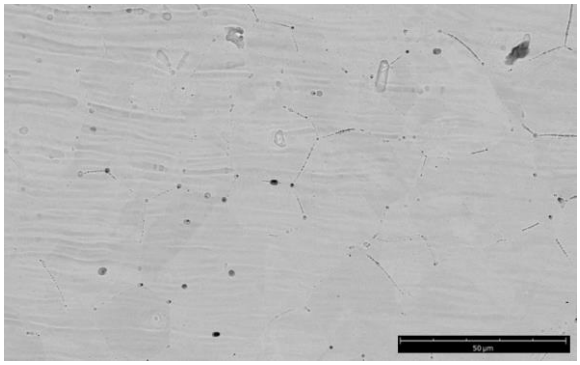

Fig. 1. Microstructure of alloyed austenite with evolved carbons at grain boundaries in AISI 310s steel in the supply state; SEM

Table 1. Chemical composition of steel AISI 310s

AISI 310s	C < 0.2	Mn < 1.5	Si < 1.0
P < 0.045	S < 0.030	Cr 22.0–25.0	Ni 17.0–20.0
Mo < 0.5	V < 0.2	W < 0.5	Fe rest

Table 2. Mechanical properties of steel AISI 310s

tensile strength Rm	Elongation A	Hardness
500–700 MPa	33%	192HB

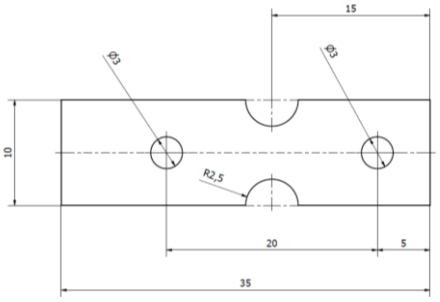

Fig. 2. Austenitic steel membrane dimensions

2.2. Methodology

Electrochemical measurements were performed using a BioLogis SP50ze potentiostat/galvanostat. The current waveforms were carried out in an electrolyte with a concentration of 0.5M H_2SO_4 acid and a pH of 1. Voltamperometry (CV measurement) was carried out in a three-electrode system, where the metallic membrane was the working electrode, the Ag/AgCl electrode was the reference electrode, and the platinum electrode was the counting electrode. The measurement procedure began with a 10-minute open circuit (OCV) measurement in the applied electrode system, on the basis of which the open circuit potential Ewe was determined, which was used to determine the range of the voltammetry process. The open circuit voltage consists of the period during which no potential or current is applied to the working electrode. The cell is disconnected from the power amplifier. Potential measurements are available on the cell. Thus, the evolution of the resting potential can be recorded. This period is commonly used as a preconditioning time or to equilibrate an electrochemical cell.

Measurements of CV voltammetry were carried out in the range below the Ewe open circuit value to eliminate the oxidation process and force the hydrogen evolution process. Cyclic voltammetry (CV) is the most pitchfork used technique for acquiring qualitative information about electrochemical reaction. CV provides information on redox processes, heterogeneous electron-transfer reactions and adsorption processes. It offers a rapid location of re-dox potential of the electroactive species. A CV consists of scanning linearly the potential of a stationary working electrode using a triangular potential waveform. During the potential sweep, the potential measures the current resulting from electrochemical reactions. The cyclic voltammogram is a current response as a function of the applied potential. The paper presents the results for two ranges of hydrogenation cycles in the voltammetry process, 25 (1 h) cycles and 50 cycles (2 h), and their influence on the microstructure and properties of steel was determined. The system was cyclically charged between the potential of –0.200 V and –1.4 V, with a scan rate of 20 mV/s.

After the hydrogenation processes, the samples were immediately tensile tested in a Deben Micro test strain gauge (Thermo Fisher Scientific), compatible with the Phenom XL scanning electron microscope. The holder enables strength tests up to 1000 N and *in-situ* observations in scanning microscope mode and all operating modes. Examination of the surface of the material after hydrogenation was also carried out with the use of scanning electron microscopy methods from the Phenom XL company. Then, microhardness measurements were carried out in accordance with PN-EN ISO 6507-1:2018-05, using the Vickers method and the Leco LM-248AT microhardness tester. The measurements were carried out with a load of 2.94 N.

3. Results and discussion

3.1. Voltammetry

Voltammetry measurements CV showed in all cycles similar shape of the curves, during observations the hydrogenation process showed an increasingly intense and violet process of hydrogen evolution in the lower parts of the

graph. The most intensive hydrogenation process took place in the range below 0.5 Ewe, numerous hydrogen bubbles were visible, concentrating on the surface of the metallic membrane constituting the working electrode. In subsequent hydrogenation cycles, the current values decreased in the range of –2.5 mA/cm to –3.5 mA/cm for 25 cycles (Fig. 3). For hydrogenation in 50 cycles, the current values were lower and oscillated from –3.0 mA/cm to –6 mA/cm (Fig. 4). Differences in the initial values result from differences in the closed-circuit measurement values in a given electrode system. There is a clear tendency to decrease the current values in successive hydrogenation cycles. This proves the changes taking place in the metallic membranes and the change of their electrochemical potentials in relation to the material in the delivery state.

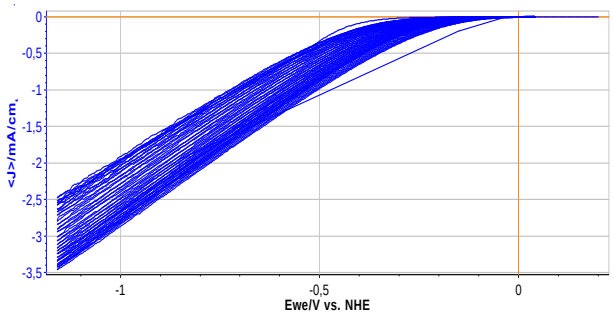

Fig. 3. Cyclic Voltammetry (CV) curve after 25 hydrogen cycles in $0.5MH_2SO_4$

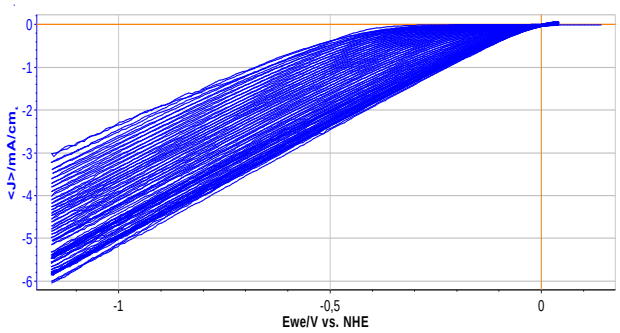

Fig. 4. Cyclic Voltammetry (CV) curve after 50 hydrogen cycles in $0.5MH_2SO_4$

3.2. Surface of membranes after hydrogenation

Observation of the surface of the metallic membranes after the hydrogenation process did not show any changes in the form of local bubbles or dissolution of alloy austenite grain boundaries. Observations indicate the lack of processes of surface degradation of metallic materials at the assumed potentiation parameters in the process of hydrogenation. The surface of the membrane, as supplied shows a texture after the treatments of the grinding process, visible in the form of parallel lines (Fig. 5). Analysis of the surface of the membranes after the hydrogenation process also showed an analogous texture and the presence of parallel lines after the grinding process (Fig. 6 and Fig. 7).

3.3. Stretch curves

The samples, after the hydrogenation process, were subjected to axial tensile testing at a constant speed of 0.5 mm/s inside a scanning electron microscope chamber equipped with a tensile holder with a maximum measurement force of 1 kN. All the tensile tests were conducted in a single setup, creating geometric notches in the central part of the samples. As a result of the tensile testing, the maximum force and elongation were determined, which were considered as comparative values due to the identical geometry of the samples (Fig. 8).

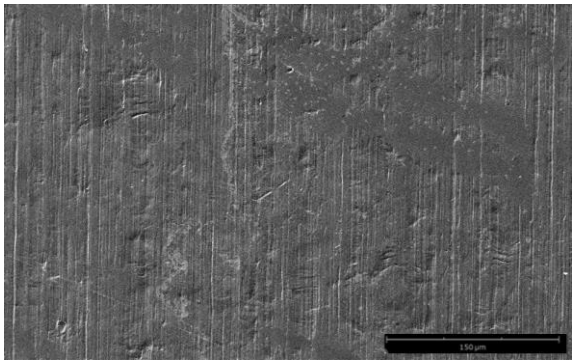

Fig. 5. Surface of AISI 310s metallic steel membrane in delivery state; SEM

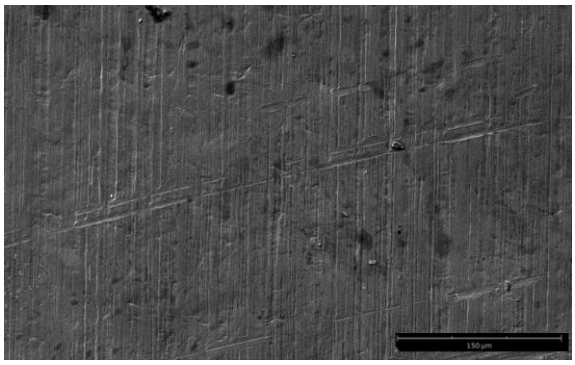

Fig. 6. Surface of AISI 310s metallic membrane after 25 cycles of hydrogenation; SEM

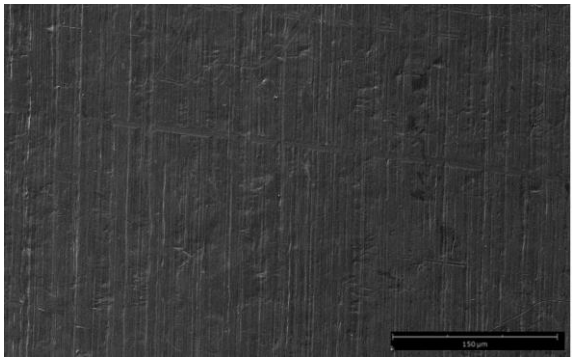

Fig. 7. Surface of AISI 310s metallic membrane after 50 cycles of hydrogenation; SEM

The hydrogenation process after 25 and 50 cycles resulted in a slight strengthening of the material, increasing the maximum force value by 3%, which represents a minor change. On the other hand, the elongation value underwent a significant reduction, decreasing by 9% after 25 cycles of hydrogenation and 13% after 50 cycles of hydrogenation compared to the reference state. This indicates a negative impact of the hydrogen environment on AISI 310S steel.

The steel becomes brittle and more prone to cracking, which can result in sudden and uncontrolled material fracture. This effect is most intense in the first hours of hydrogenation [26, 27].

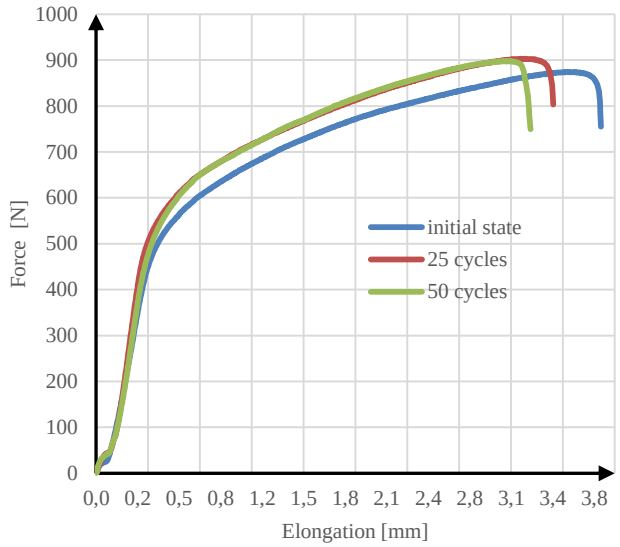

Fig. 8. Tensile curves for delivery state AISI 310s, hydrogenation after 25 cycles and 50 cycles

3.4. Fractographic observations

Fractographic examination of the surface of the material, both in the initial state and after the hydrogenation process, showed the characteristics of plastic fracture. No areas of hydrogen embrittlement are visible in any area. Due to the high degree of elongation of the sample, the observed fracture belongs to ductile fractures. The surface of the membrane in the area at the fracture focus shows the presence of numerous irregular plastic striations parallel to the crack front (Fig. 9, 11 and 13). The location of the stripes coincides with the texture after surface treatment and is a mirror image of the scratches from the abrasive papers, which are the places of their formation initiation. It has been observed that striations appear during the stretching of the membranes from the initial stages of strain. Fractographic examinations of fractures show clear changes, which indicate the formation of a plastic fracture. Dimples of various sizes are visible, and typical sliding cracks with fine scales are also visible (Fig. 10, 12 and 14).

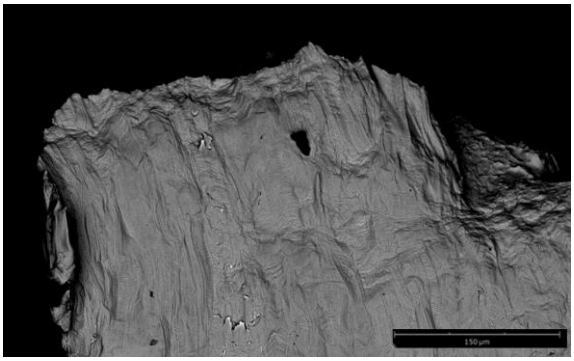

Fig. 9. Plastic breakthrough of the membrane in the state of delivery AISI 310s; SEM

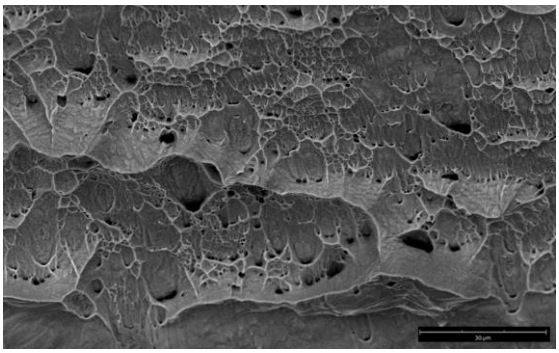

Fig. 10. Fractography breakthrough material in the state of delivery AISI 310s; SEM

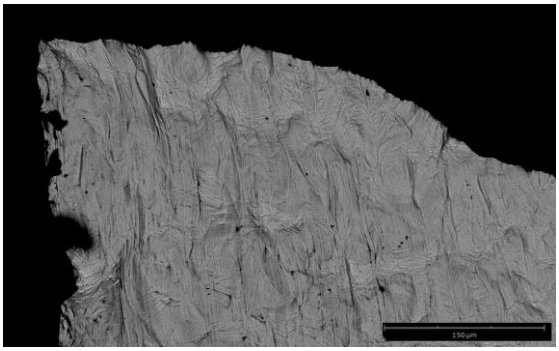

Fig. 11. Plastic membrane breakthrough after hydrogenation after 25 cycles; SEM

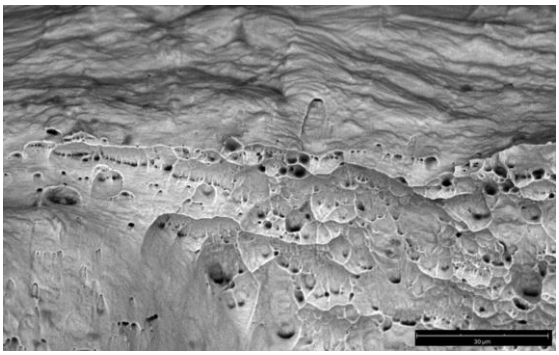

Fig. 12. Fractography of material breakthrough after hydrogenation after 25 cycles; SEM

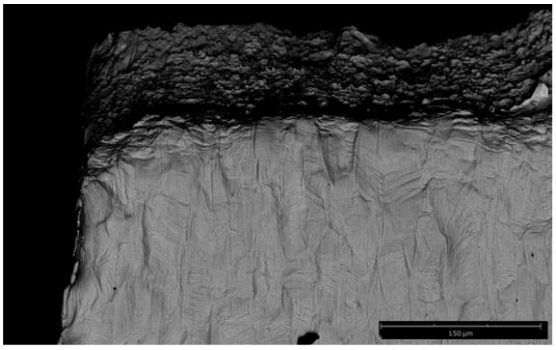

Fig. 13. Plastic membrane breakthrough after hydrogenation after 50 cycles; SEM

Grain boundaries and numerous micropores formed in places of stress concentration are clearly outlined. Crystal lattice defects, usually dislocations, which form clusters on

obstacles blocking their movement, play a large role in the formation of micropores. As the plastic deformation progressed, the micropores grew larger and closer together. Bridges were formed in these areas, which formed fibrils as a result of thinning, the resulting fractures have the characteristics of fibrous fractures.

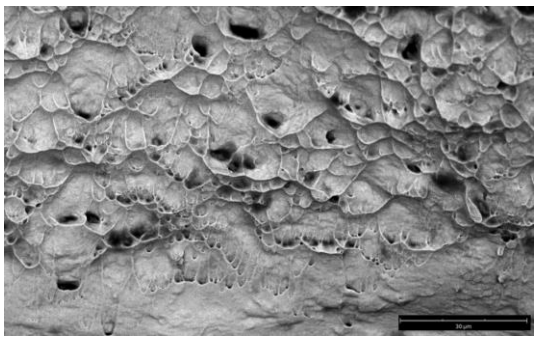

Fig. 14. Fractography of material breakthrough after hydrogenation after 25 cycles; SEM

3.5. Hardness measurements

Microhardness tests are one of the simplest methods to determine changes in the form of strengthening in the material after the hydrogenation process. Hardness measurements were carried out on the surface of the membranes, on the undeformed elements of the sample after the hydrogenation process. Analysis of the microhardness results showed that the H_2 environment affects the surface hardening of AISI 310s steel (Fig. 15). The increase in the microhardness value is directly proportional to the cycles of electrolytic hydrogenation. Before the hydrogenation process, the average hardness of the material as supplied was 154 HV0.2. The results of the hydrogenation showed an increase in hardness for the membranes after 25 cycles to an average value of 163 HV0.2. The highest value increase was obtained with the longest exposure of the material to hydrogen, after 50 cycles the hardness increased to 170HV0.2.

4. Conclusion

The presented paper presents the process of hydrogen loading membranes of AISI 310s austenitic steel in order to assess the influence of hydrogen on the properties of this steel. Based on the test results, it was found that the material was strengthened by the process of electrochemical hydrogenation in 0.5M H_2SO_4 solution. The increase in strengthening is directly proportional to the amount of hydrogen supplied to the material (number of cycles), confirmed by strength tests and hardness measurements. This indicates a negative impact of the hydrogen environment on AISI 310S steel. The steel becomes brittle and more prone to cracking, which can result in sudden and uncontrolled material fracture. This is likely due to the diffusion of hydrogen into the material, which causes changes in the material's crystal structure and mechanical properties. As a result, the internally remodeled material has a greater tendency to strengthen and crack under load. The occurrence of the features of the form of hydrogen embrittlement known from the literature in the form of local brittle fracture zones was not observed in any of the materials.

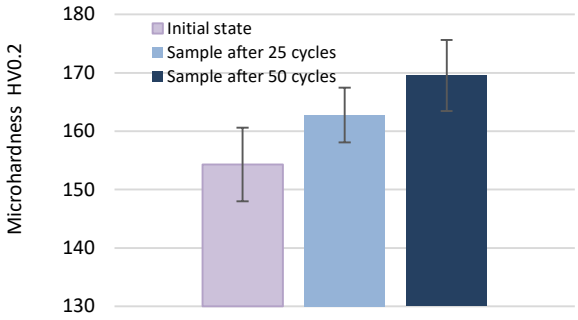

Fig. 15. Averaged results of material hardness in the delivery state, after 25 cycles and 50 hydrogenation cycles

Based on the research, it was found that the process of cathodic hydrogen charging in the electrolytic process in a solution of 0.5MH_2SO_4 significantly affects the strengthening of AISI 310s steel, while maintaining the plastic character of the breakthrough. No areas of brittle fractures characteristic of hydrogen embrittlement were found in fractographic studies. Additively, the presence of carbides at grain boundaries can act as areas of stress concentration, which can increase susceptibility to hydrogen embrittlement in these areas. Where carbides are present, hydrogen can accumulate more easily and lead to localized weakening of the material's structure. However, this mechanism was not confirmed in the study.

Acknowledgements

The work was carried out as part of a funding project from the National Science Centre Miniatura 6 with the number 02NA/0005/22. We would also like to thank PIK Instruments and Termo Fisher Scientific for providing the research equipment.

Bibliography

[1] Au M. Mechanical behavior and fractography of 304 stainless steel with high hydrogen concentration. No WSRC-TR-2002-00558 Savannah River Site (US). 2003;865. https://www.osti.gov/servlets/purl/807672

[2] Bertsch KM, Nagao A, Rankouhi B, Kuehl B, Thoma DJ. Hydrogen embrittlement of additively manufactured austenitic stainless steel 316 L. Corros Sci. 2021;192:109790. https://doi.org/10.1016/j.corsci.2021.109790

[3] Caskey GR. Fractography of hydrogen-embrittled stainless steel. Scripta Metallurgica. 1977;11(12):1077-1083. https://doi.org/10.1016/0036-9748(77)90311-8

[4] Das T, Legrand E, Brahimi SV, Song J, Yue S. Evaluation of material susceptibility to hydrogen embrittlement (HE): an approach based on experimental and finite element (FE) analyses. Eng Fract Mech. 2020;224:106714. https://doi.org/10.1016/j.engfracmech.2019.106714

[5] Gavriljuk VG, Hänninen H, Tarasenko AV, Tereshchenko AS, Ullakko K. Phase transformations and relaxation phenomena caused by hydrogen in stable austenitic stainless steels. Acta Metallurgica et Materialia. 1995;43(2):559-568. https://doi.org/10.1002/9781118803363.ch78

[6] Hamaad ASAA, Tawfik M, Khattab S, Newir A. Device for using hydrogen gas as environmental friendly fuel for automotive engine (GREEN & ECO H2). Procedia Environ Sci. 2017;37:564-571. https://doi.org/10.1016/j.proenv.2017.03.043
[7] Hatano M, Fujinami M, Arai K, Fujii H, Nagumo M. Hydrogen embrittlement of austenitic stainless steels revealed by deformation microstructures and strain-induced creation of vacancies. Acta Mater. 2014;67:342-353. https://doi.org/10.1016/j.actamat.2013.12.039
[8] Khanchandani H, Gault B. Atomic scale understanding of the role of hydrogen and oxygen segregation in the embrittlement of grain boundaries in a twinning induced plasticity steel. Scr Mater. 2023;234:115593. https://doi.org/10.1016/j.scriptamat.2023.115593
[9] Kim HP, Park YM, Jang HM, Lim SY, Choi MJ, Kim SW et al. Early-stage M23C6 morphology at the phase boundary in type 304L austenitic stainless steel containing δ ferrite. Metals. 2022;12(11):1794. https://doi.org/10.3390/met12111794
[10] Komatsu A, Fujinami M, Hatano M, Matsumoto K, Sugeoi M, Chiari L. Straining-temperature dependence of vacancy behavior in hydrogen-charged austenitic stainless steel 316L. Int J Hydrogen Energy. 2021;46(9):6960-6969. https://doi.org/10.1016/j.ijhydene.2020.11.148
[11] Lai CL, Tsay LW, Chen C. Effect of microstructure on hydrogen embrittlement of various stainless steels. Materials Science and Engineering: A. 2013;584:14-20. https://doi.org/10.1016/j.msea.2013.07.004
[12] Lang F, Huang F, Yue J, Li L, Xu J, Liu J. Hydrogen trapping and hydrogen embrittlement (HE) susceptibility of X70 grade high-strength, acid-resistant, submarine pipeline steel with Mg treatment. Journal of Materials Research and Technology. 2023;24:623-638. https://doi.org/10.1016/J.JMRT.2023.03.011
[13] Li X, Ma X, Zhang J, Akiyama E, Wang Y, Song X. Review of hydrogen embrittlement in metals: hydrogen diffusion, hydrogen characterization, hydrogen embrittlement mechanism and prevention. Acta Metallurgica Sinica (English Letters). 2020;33:759-773. https://doi.org/10.1007/s40195-020-01039-7
[14] Longwic R, Tatarynow D, Kuszneruk M, Wozniak-Borawska G. Preliminary tests of a Diesel engine powered by diesel and hydrogen. Combustion Engines. 2023;195(4):35-39. https://doi.org/10.19206/CE-169485
[15] Mamala J, Graba M, Mitrovic J, Prażnowski K, Stasiak P. Analysis of speed limit and energy consumption in electric vehicles. Combustion Engines. 2023;195(4):83-89. https://doi.org/10.19206/CE-169370
[16] Matsuo T, Yamabe J, Matsuoka S. Effects of hydrogen on tensile properties and fracture surface morphologies of type 316L stainless steel. Int J Hydrogen Energy. 2014;39(7):3542-3551. https://doi.org/10.1016/j.ijhydene.2013.12.099
[17] Nicho K, Yokoyama K. Marked degradation of tensile properties induced by plastic deformation after interactions between strain-induced martensite transformation and hydrogen for type 316L stainless steel. Metals. 2020;10(7):928. https://doi.org/10.3390/met10070928
[18] Rieck RM, Atrens A, Smith IO. Stress corrosion cracking and hydrogen embrittlement of cold worked AISI type 304 austenitic stainless steel in mode I and mode III. Materials Science and Technology. 1986;2(10):1066-1073. https://doi.org/10.1179/mst.1986.2.10.1066
[19] Saborío-González M, Rojas-Hernández I. Review: hydrogen embrittlement of metals and alloys in combustion engines. Revista Tecnología en Marcha. 2018;31(2). https://doi.org/10.18845/tm.v31i2.3620
[20] Safyari M, Khossossi N, Meisel T, Dey P, Prohaska T, Moshtaghi M. New insights into hydrogen trapping and embrittlement in high strength aluminum alloys. Corros Sci. 2023;223:111453. https://doi.org/10.1016/J.CORSCI.2023.111453
[21] Tomaszewski S, Grygier D, Dziubek M. Assessment of engine valve materials. Combustion Engines. 2023;194(3):48-51. https://doi.org/10.19206/CE-166569
[22] Toribio J, Lorenzo M, Aguado L. Innovative design of residual stress and strain distributions for analyzing the hydrogen embrittlement phenomenon in metallic materials. Materials. 2022;15(24):9063. https://doi.org/10.3390/ma15249063
[23] Verhelst S, Wallner T. Hydrogen-fueled internal combustion engines. Progress in Energy and Combustion Science. 2009;35(6):490-527. https://doi.org/10.1016/j.pecs.2009.08.001
[24] Wang L, Fang X, Wang J, Zhang Z. The precipitation control of grain boundary M23C6 phases and the ductility improvement in aged 22Cr-25Ni-WCuNbN austenitic stainless steel by Co addition. Mater Lett. 2020;264:127348. https://doi.org/10.1016/j.matlet.2020.127348
[25] Wang Y, Wang X, Gong J, Shen L, Dong W. Hydrogen embrittlement of catholically hydrogen-precharged 304L austenitic stainless steel: effect of plastic pre-strain. Int J Hydrogen Energy. 2014;39(25):13909-13918. https://doi.org/10.1016/j.ijhydene.2014.04.122
[26] Wu X, Zhang H, Yang M, Jia W, Qiu Y, Lan L. From the perspective of new technology of blending hydrogen into natural gas pipelines transmission: mechanism, experimental study, and suggestions for further work of hydrogen embrittlement in high-strength pipeline steels. Int J Hydrogen Energ. 2022;47(12):8071-8090. https://doi.org/10.1016/j.ijhydene.2021.12.108
[27] Xue J, Wu H, Zhou C, Zhang Y, He M, Yan X et al. Effect of heat input on hydrogen embrittlement of TIG welded 304 austenitic stainless steel. Metals. 2022;12(11):1943. https://doi.org/10.3390/met12111943
[28] Ye F, Zhu T, Mori K, Xu Q, Song Y, Wang Q et al. Effects of dislocations and hydrogen concentration on hydrogen embrittlement of austenitic 316 stainless steels. J Alloys Compd. 2021;876:160134. https://doi.org/10.1016/j.jallcom.2021.160134

Malgorzata Rutkowska-Gorczyca, DEng. – Faculty of Mechanical Engineering, Wroclaw University of Science and Technology. Poland.
e-mail: *malgorzata.rutkowska-gorczyca@pwr.edu.pl*

Mateusz Dziubek, MEng. – Faculty of Mechanical Engineering, Wroclaw University of Science and Technology. Poland.
e-mail: *mateusz.dziubek@pwr.edu.pl*

Marcin Wiśniewski, Eng. – student research group of Materials Science, Mechanical Engineering, Wroclaw University of Science and Technology, Poland.
e-mail: *255206@student.pwr.edu.pl*